

High-temperature magnetic behavior of FeCo-based nanocrystalline alloys

C. Gómez-Polo,* J. I. Pérez-Landazabal, and V. Recarte

Departamento de Física, Universidad Pública de Navarra, Campus de Arrosadia, 31006 Pamplona, Spain

J. Campo

Institut Laue Langevin, Boîte Postal 156, 6 rue J. Horowitz, 38000 Grenoble, France

P. Marín, M. López, and A. Hernando

Instituto de Magnetismo Aplicado (UCM-RENFÉ), P.O. Box 155, 28230 Las Rozas, Spain

M. Vázquez

Instituto de Ciencia de Materiales, CSIC, Campus de Cantoblanco, 28049 Madrid, Spain

(Received 11 February 2002; published 20 June 2002)

The soft magnetic response of nanocrystalline $\text{Fe}_{73.5-x}\text{Co}_x\text{Si}_{13.5}\text{B}_9\text{Cu}_1\text{Nb}_3$ ($x=0, 30, \text{ and } 45$) samples are analyzed above room temperature through the temperature evolution of the magnetic permeability and the associated loss factor. Moreover, the actual structure and composition of the crystalline phase is analyzed through neutron-diffraction studies. The results show that the inclusion of Co atoms give rise to an improvement in the soft magnetic behavior at high temperatures with respect to the Fe-based sample as a consequence of the increase in the Curie temperature of the precipitated crystallites. However, the role of the residual amorphous matrix cannot be disregarded and the decrease in its Curie temperature for the Co richest sample gives rise to a deterioration of the high-temperature soft magnetic response. The observed temperature evolution is analyzed within the framework of the random anisotropy model and associated with the temperature dependence of the magnetic coupling between the ferromagnetic crystals.

DOI: 10.1103/PhysRevB.66.012401

PACS number(s): 75.50.Tt, 75.50.Bb, 75.30.Cr, 75.30.Et

The study of FeCo-based nanocrystalline materials represents a topic of growing interest in the field of new bulk soft magnetic materials for high-temperature applications.¹⁻¹⁰ These nanocrystalline materials are characterized by the precipitation of a randomly oriented FeCo nanocrystals embedded in a residual amorphous matrix. Their excellent soft magnetic response is mainly correlated with the averaging out of the magnetocrystalline anisotropy via the magnetic interactions between the two constituent magnetic phases. In these FeCo-based nanocrystalline alloys, the higher saturation magnetization and Curie temperature of the crystalline phase with respect to the Fe based alloys, determines their high-temperature magnetic response and makes them promising candidates to be extensively employed in high-temperature power applications.

Among these FeCo nanocrystalline alloys the FeCoZrBCu alloys (HITPERM) stand out.¹⁻⁵ In these alloys the precipitation of the cubic FeCo grains (*B2* structure) bear an improvement of the high-temperature soft magnetic properties with respect to the Fe based FeBCuM ($M = \text{Zr, Nb, Hf}$) alloys. In a similar way, when Co is added to the FeSiBNbCu alloys, a different FeCo(Si) crystalline phase characterizes the nanocrystalline state.⁶⁻¹⁰ Due to its higher magnetic moment and Curie temperature with respect to the FeSi phase a similar improvement of the soft magnetic response at high temperatures must be expected. However, the magnetic nature and temperature dependence of the residual amorphous matrix should not be disregarded and its contribution at high temperatures could play a dominant role in the magnetic coupling between the two ferromagnetic phases. In this sense, the aim of the present work is to analyze the temperature

dependence of the magnetic coupling in nanocrystalline $\text{Fe}_{73.5-x}\text{Co}_x\text{Si}_{13.5}\text{B}_9\text{Cu}_1\text{Nb}_3$ alloys through the analysis of the temperature evolution of the magnetic permeability.

Amorphous ribbons 1 mm wide, about 20 μm thick, were obtained by melt spinning technique with nominal composition $\text{Fe}_{73.5-x}\text{Co}_x\text{Si}_{13.5}\text{B}_9\text{Cu}_1\text{Nb}_3$ ($x=0, 30, \text{ and } 45$). In order to obtain the characteristic nanocrystalline structure, the samples were submitted to isothermal treatments (1 h) in an Ar atmosphere at 550 °C. The precipitated crystalline phase was analyzed by room-temperature neutron-diffraction measurements at the D1B diffractometer in the Institut Laue Langevin (ILL), Grenoble (France). The radiation employed ($\lambda = 1.28 \text{ \AA}$) was monochromatized using germanium with the (3,1,1) reflection. Transmission data were collected from $2\theta = 10^\circ - 90^\circ$ in 0.2° steps with a $^3\text{He/Xe}$ position sensitive detector. The actual structure of the precipitated crystalline phase was analyzed through the fitting of the obtained spectra using the Rietveld method,^{11,12} through the FULLPROF98 program.¹³ Background corrections were performed with a fourth-order polynomial function and the peak profile parameters were refined assuming a Gaussian profile. With respect to the magnetic measurements, the temperature dependence of the magnetic permeability was determined through a conventional induction method at 1 kHz, with a maximum ac magnetic field of 48 A/m in a temperature range from 200 to 475 °C. The room-temperature axial hysteresis loops at 50 Hz were also obtained in order to estimate the coercivity of the as-cast and annealed samples.

Figure 1 shows the room-temperature neutron-diffraction patterns for the annealed $\text{Fe}_{73.5-x}\text{Co}_x\text{Si}_{13.5}\text{B}_9\text{Cu}_1\text{Nb}_3$ alloys with $x=0$ (a) and $x=45$ (b). Both alloys are characterized by

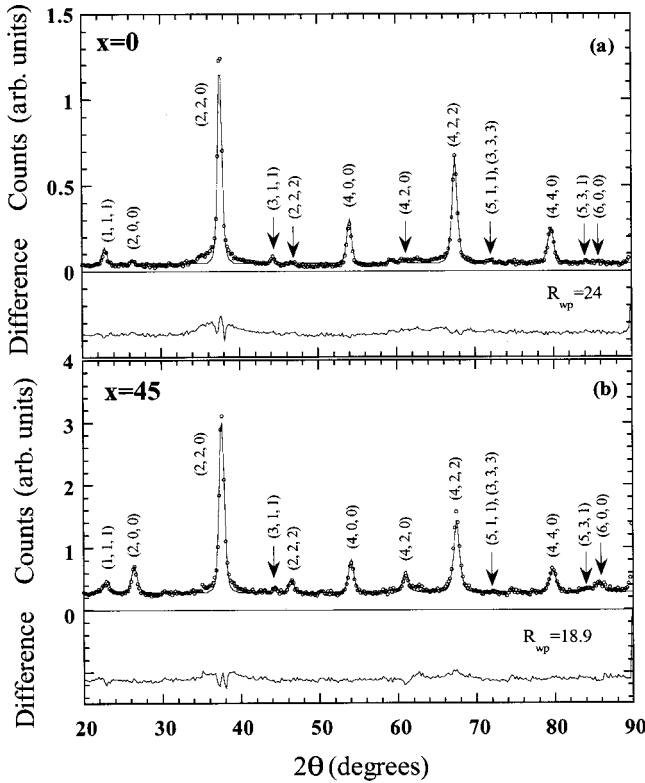


FIG. 1. Room-temperature neutron-diffraction patterns for the nanocrystalline $\text{Fe}_{73.5-x}\text{Co}_x\text{Si}_{13.5}\text{B}_9\text{Cu}_1\text{Nb}_3$ samples ($T_a = 550^\circ\text{C}$, 1 h) for (a) $x=0$ and (b) $x=45$. The solid line represents the Rietveld refinement. The standard difference between the measured and calculated profiles is shown at the bottom of the diagram.

the precipitation of a randomly oriented fcc phase with mean grain diameter of the order of tens of nanometers. As it is extensively reported, the Fe-based sample ($x=0$) is characterized by the precipitation of the Fe_3Si with DO_3 superstructure (lattice parameter, $a = 5.667 \text{ \AA}$).¹⁴ In this structure Fe atoms are located at two nonequivalent $(\frac{1}{4}, \frac{1}{4}, \frac{1}{4})$ and $(\frac{1}{2}, \frac{1}{2}, \frac{1}{2})$ positions (8c and 4b, respectively, according Wyckoff notation, International tables of Crystallography)¹⁵ and Si atoms in the (0, 0, 0) positions (4a). It has been shown that when transition metal impurities are added to Fe_3Si , there is a selective substitution for Fe in one of the two nonequivalent sites depending on the position of the impurities in the periodic table.^{16,17} In the particular case of Co, nuclear-magnetic-resonance, neutron-diffraction, and Mössbauer experiments show that Co substitutes Fe into the 8c positions, forming a single fcc phase ($\text{Fe}_{3-y}\text{Co}_y\text{Si}$) for $y \leq 2.15$.

In our present case, the effect of the inclusion of Co can be first observed through the analysis of the superstructure (1,1,1) and (2,0,0) reflections of the neutron-diffraction spectra. As Fig. 1 shows the inclusion of Co gives rise to a clear change in the relative intensities of both reflections that can be directly ascribed to the inclusion of Co atoms in the precipitated crystalline phase. This effect cannot be observed by conventional x-ray diffraction experiments due to the similar values of the x-ray scattering factors for Fe and Co atoms. Using the Rietveld refinement technique, the estimation of

TABLE I. Room temperature coercivity, H_C (50 Hz), for $x=0$, 30, and 45 nanocrystalline $\text{Fe}_{73.5-x}\text{Co}_x\text{Si}_{13.5}\text{B}_9\text{Cu}_1\text{Nb}_3$ samples.

x	$H_C(\text{A/m})$	$H_C(\text{A/m})$
	As-cast	Annealed
0	8.6	3.6
30	2.4	10.7
45	4.8	14.8

the actual structure of the crystalline phase can be performed. The solid line in Figs. 1(a) and 1(b) show the Rietveld refinement to the DO_3 and $L2_1$ superstructures, respectively, with the following magnetic moments: μ (Fe_I , in 4b positions) = $2.20\mu_B$, μ (Fe_{II} , in 8c positions) = $1.35\mu_B$, μ (Co) = $1.70\mu_B$ and μ (Si) = $-0.07\mu_B$ (Ref. 16) (global temperature factor $B = (0.35 \pm 0.05) \text{ \AA}^2$ and magnetic moments parallel to the cubic axis). The best fitting is obtained assuming the previous Co substitution into the 8c positions and the following compositions: $x=0$, $\text{Fe}_{80}\text{Si}_{20}$ and $x=45$, $\text{Fe}_{35}\text{Co}_{50}\text{Si}_{15}$. It is important to remark that the presented neutron-diffraction studies confirm the previously reported compositional dependence obtained from the comparison between the decrease of the lattice parameter of the precipitated crystalline phase with x (x-ray diffractometry) in these nanocrystalline samples and the reported data in $\text{Fe}_{3-y}\text{Co}_y\text{Si}$ crystalline alloys.¹⁰

With respect to the magnetic measurements, Table I summarizes the room-temperature coercivity, H_C , for the samples in as-cast state and after being submitted to the nanocrystallization thermal treatment. An intermediate composition with $x=30$ is also included. As these results reflect, the optimum soft magnetic state at room temperature is found in the annealed sample for $x=0$. However, in the FeCo alloys the crystallization process gives rise to an increase of H_C with respect to as-cast value. The detected increase of H_C with x must be correlated with the increase in the mean grain diameter, d , of the precipitated crystalline phase [from $d(x=0) = 11$ to $d(x=45) = 15 \text{ nm}$] as previous x-ray diffraction and transmission electron microscopy studies reflect.¹⁰

In order to characterize the high-temperature magnetic response of the nanocrystalline alloys, the magnetic permeability, μ , was measured as a function of the temperature, T , ($200 \leq T \leq 475^\circ\text{C}$). Figure 2 shows the temperature dependence of the (a) real (μ_r) and (b) imaginary (μ_i) components of the magnetic permeability, $\mu = \mu_r + i\mu_i$, for $x=0$, 30, and 45. First, the inclusion of Co atoms in the nominal composition of the alloy ($x=30$ and 45) gives rise for low measuring temperatures ($T \leq 225^\circ\text{C}$) to a decrease and an increase of μ_r and μ_i , respectively, with respect to the permeability of the Fe-based sample ($x=0$). This magnetic hardening supports the presented evolution of the room-temperature coercivity, H_C , displayed in Table I. However, the most remarkable result regarding high-temperature applications is that the FeCo samples present an increase in the magnetic response (increase in μ) for $T > 300^\circ\text{C}$ with respect to that of Fe-based alloy ($x=0$). As is shown in Ref. 10, an increase in the nominal Co content of the alloy, x ,

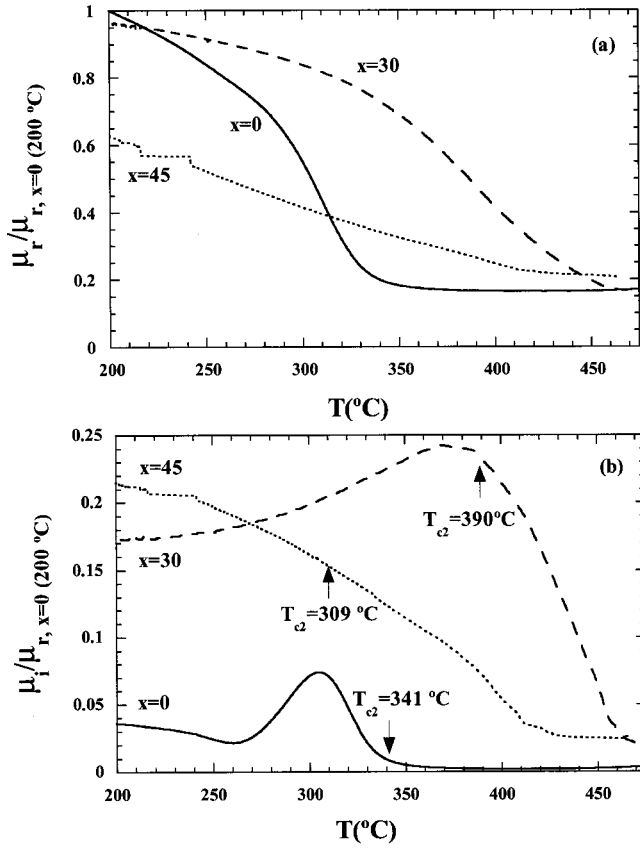


FIG. 2. Temperature (T) dependence of the (a) real (μ_r) and (b) imaginary (μ_i) components of the magnetic permeability, $\mu = \mu_r + i\mu_i$ for $x=0, 30,$ and 45 nanocrystalline $\text{Fe}_{73.5-x}\text{Co}_x\text{Si}_{13.5}\text{B}_9\text{Cu}_1\text{Nb}_3$ samples. The Curie temperature of the residual amorphous matrix, T_{C2} , are indicated with arrows in (b).

gives rise to an enrichment of Co concentration in the precipitated crystalline phase and to a parallel increase in its corresponding Curie temperature [i.e., T_{C1} [$T_{C1}(x=0) = 530^\circ\text{C}$ and $T_{C1}(x=45) = 796^\circ\text{C}$]]. Thus, if the crystalline phase dominates the high-temperature magnetic behavior, this increase of T_{C1} with the Co content of the crystalline phase will have associated a parallel increase in μ at high temperatures. However, as Fig. 2 shows, the highest magnetic response at $T > 300^\circ\text{C}$ is obtained for $x=30$ instead of $x=45$ (the Co richest sample). Then, the role of the residual amorphous matrix cannot be disregarded and must be analyzed in order to explain the observed high-temperature μ behavior.

As Fig. 2(b) shows, where the Curie points of the residual amorphous matrix, T_{C2} , obtained from previous thermogravimetry analysis¹⁰ are indicated with arrows, the imaginary component, μ_i presents a maximum value for $T \approx T_{C2}$. Such a maximum is a characteristic feature of different magnetic transitions (i.e., freezing temperature in spin glasses¹⁸). Due to the proximity of T_{C2} , this maximum can be ascribed in our present case to the magnetic decoupling between ferromagnetic crystallites. However, it is remarkable that in the Co richest sample ($x=45$) μ_i just smoothly decreases with T .

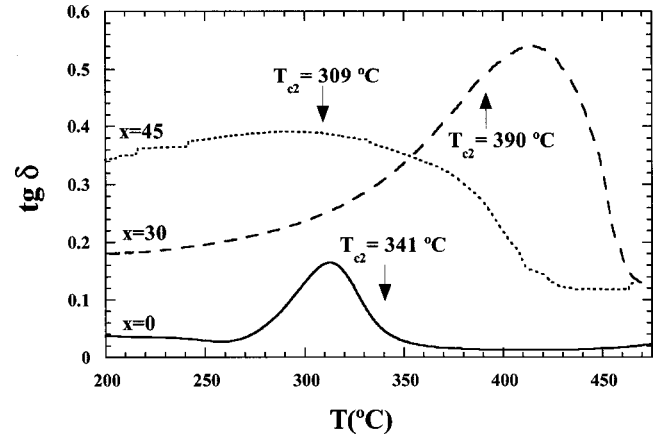


FIG. 3. Loss factor, $tg \delta$, versus temperature, T , for $x=0, 30,$ and 45 nanocrystalline $\text{Fe}_{73.5-x}\text{Co}_x\text{Si}_{13.5}\text{B}_9\text{Cu}_1\text{Nb}_3$ samples. The Curie temperatures of the residual amorphous matrix, T_{C2} , are indicated with arrows.

To characterize this magnetic transition the loss factor $tg \delta$ is introduced as

$$tg \delta = \frac{\mu_i}{\mu_r}. \quad (1)$$

Figure 3 shows the temperature dependence of $tg \delta$ for the analyzed nanocrystalline samples. Since $tg \delta$ is associated to the energy loss per cycle, its maximum value around T_{C2} can be directly ascribed to the magnetic decoupling between ferromagnetic crystallites. In fact, the occurrence of maximum values in $H_c(T)$ for $T \approx T_{C2}$ in similar nanocrystalline systems is extensively reported and correlated to the magnetic transition associated to the magnetic decoupling between crystallites.^{19,20}

First, for $x=45$ a wide maximum in $tg \delta$ is found for $T \approx T_{C2}$. The occurrence of broad maximums in $H_c(T)$ in these nanocrystalline systems has been previously reported and associated to the existence of a broad distribution of Curie temperatures of the residual amorphous matrix.^{19–21} Then, the observed increase in the width of the maximum of $tg \delta$ with x (see Fig. 3), would indicate a parallel increase in the inhomogeneity of the residual amorphous phase. For $x=45$ this inhomogeneous contribution would give rise to the absence of a well-defined transition temperature and thus to the disappearance of the maximum value in $\mu_i(T)$ [see Fig. 2(b)].

Second, it is important to remark that the temperature of the maximum in $tg \delta$, T_P , does not agree with T_{C2} for $x=0$ and 30 samples (see Fig. 3). While $T_P < T_{C2}$ for $x=0$, the opposite behavior ($T_P > T_{C2}$) is found for $x=30$. As was previously shown,²² within the framework of the random anisotropy model, the temperature dependence of the effective magnetocrystalline anisotropy, k_{eff} can be expressed as

$$k_{\text{eff}} = \frac{v_c^2 k_1^4 d^6}{A^3} \quad (2)$$

with v_c being the volume crystalline fraction, k_1 being the magnetocrystalline constant of the crystalline phase, and A

being the mean exchange constant of the coupled system, $A = (A_1 A_2)^{1/2}$ (A_1 and A_2 the exchange constants of the crystalline and amorphous phases). Assuming k_1 and A_1 to be roughly constants in the measuring temperature range, $k_{\text{eff}}(T)$ should increase as a consequence of the expected decrease of A_2 for $T \leq T_{C2}$. The magnetic decoupling between the ferromagnetic grains would take place at a temperature T_P where $k_{\text{eff}}(T_P) \approx k_1$. Therefore, according to Eq. (2), T_P and the temperature evolution of $k_{\text{eff}}(T)$ would be mainly governed by $A_2(T)$.^{23,24} Considering $A_2(T) \propto (1 - T/T_{C2})^{2\beta}$ ($\beta = 0.36$) near T_{C2} , it is quite clear that the magnetic decoupling should be always observed for $T \leq T_{C2}$ ($x = 0$ and 45 samples). However, as it is shown in Fig. 3, the magnetic transition takes place for $x = 30$ above the Curie temperature of the amorphous matrix. The shift in T_P above T_{C2} can only be explained assuming that the exchange coupling between grains takes place through the paramagnetic amorphous matrix,^{19,20,25} as is extensively reported in multilayered systems.²⁶ In our present case, due to the similar main distance between ferromagnetic crystals (similar mean grain sizes and volume fraction of the precipitated crystalline phase), the actual magnetization of the single ferromagnetic grains would play a dominant role in the occurrence of the shift of T_P above T_{C2} for $x = 30$. In this sense, high-temperature studies are now in progress in order to deepen into the exchange interaction contribution to this magnetic transition.

Finally, with respect to the comparison of the magnetic response with the Co content of the alloy, x , it can be concluded that the softest magnetic response is the result of the combination of the magnetic characteristics of both ferromagnetic phases. According to Eq. (2), the increase of μ (decrease of k_{eff}) for the CoFe-based samples at high temperatures should be interpreted as a consequence of the enhancement of the effective exchange correlation length, A , with respect to the Fe base ($x = 0$) alloy. At a fixed measur-

ing temperature, the exchange constant can be considered roughly proportional to the corresponding Curie temperature of each ferromagnetic phase ($A_i \propto T_{Ci}$, $i = 1, 2$). Thus, the observed increase of μ in the CoFe samples should be directly correlated to the increase in A_1 associated to the higher Curie point of the crystalline phase in these alloys. Such an enhancement is reinforced for $x = 30$ by the highest T_{C2} . However, in the Co richest sample ($x = 45$) the increase in A_1 is compensated by the parallel decrease in A_2 correlated with the decrease in the Curie temperature of the residual amorphous matrix.

In conclusion, the high-temperature evolution ($200 \leq T \leq 475$ °C) of the soft magnetic behavior of nanocrystalline $\text{Fe}_{73.5-x}\text{Co}_x\text{Si}_{13.5}\text{B}_9\text{Cu}_1\text{Nb}_3$ ($x = 0, 30$, and 45) alloys has been analyzed through the temperature dependence of the magnetic permeability and the associated loss factor. The FeCo samples present an improvement in the soft magnetic behavior for $T \geq 300$ °C, which is a direct consequence of the precipitation of a $L2_1$ -FeCoSi phase with higher Curie temperature than the DO_3 -FeSi phase characteristic of the Fe-based sample. The actual composition and structure of this precipitated crystalline phase is analyzed through neutron-diffraction studies. However, the role of the residual amorphous matrix cannot be disregarded and the decrease of its Curie point for the Co richest sample, gives rise to a decrease in the soft magnetic response at high temperatures. Thus, the results show that in the search of bulk soft magnetic materials for high-temperature applications, both crystalline and residual amorphous phase contributions must be considered in order to optimize the magnetic response in the desired high-temperature range.

This work was supported by the Spanish "Ministerio de Ciencia y Tecnología" under Project No. MAT-1999-0422-C02. The Spanish part of the D1B Collaborative Research Group, at the ILL (Grenoble, France) is acknowledged for the allocated neutron beam time (Exp CRG-474).

*Email address: gpolo@unavarra.es

¹M. A. Willard, *et al.* J. Appl. Phys. **85**, 4421 (1999).

²S. He *et al.*, J. Appl. Phys. **86**, 6301 (1999).

³T. Kemény *et al.*, Appl. Phys. Lett. **76**, 2110 (2000).

⁴M. A. Willard *et al.*, D. E. Laughlin, and M. E. McHenry, J. Appl. Phys. **87**, 7091 (2000).

⁵A. C. Hsiao *et al.*, IEEE Trans. Magn. **31**, 2236 (2001).

⁶M. Müller *et al.*, J. Magn. Magn. Mater. **160**, 284 (1996).

⁷J. Zbroszczyk *et al.*, J. Magn. Magn. Mater. **160**, 281 (1996).

⁸L. Pascual *et al.*, J. Magn. Magn. Mater. **203**, 79 (1999).

⁹J. M. Borrego *et al.*, J. Non-Cryst. Solids **287**, 120 (2001).

¹⁰C. Gómez-Polo *et al.*, Phys. Rev. B **65**, 024433 (2002).

¹¹H. M. Rietveld, J. Appl. Crystallogr. **2**, 65 (1969).

¹²R. A. Young, *The Rietveld Method* (Oxford Science, Oxford (1993)).

¹³J. Rodríguez-Cravajal, Physica B **192**, 55 (1993).

¹⁴G. Herzer, J. Magn. Magn. Mater. **112**, 258 (1992).

¹⁵*International Tables of Crystallography*, edited by T. Hand (Kluwer Academic, Dordrecht, 1996), Vol. 1.

¹⁶V. Niculescu *et al.*, Phys. Rev. B **19**, 452 (1979).

¹⁷V. A. Niculescu *et al.*, J. Magn. Magn. Mater. **39**, 223 (1983).

¹⁸D. Hüser *et al.*, Phys. Rev. B **27**, 3100 (1983).

¹⁹A. Slawska-Wanieska *et al.*, Phys. Rev. B **50**, 6465 (1994).

²⁰A. Hernando and T. Kulik, Phys. Rev. B **49**, 7064 (1994).

²¹J. S. Garitaonandia *et al.*, Phys. Rev. B **58**, 12 147 (1998).

²²J. Arcas *et al.*, Phys. Rev. B **58**, 5193 (1998).

²³K. Suzuki and J. M. Cadogan, Phys. Rev. B **58**, 2730 (1998).

²⁴A. Hernando *et al.*, Phys. Rev. B **58**, 366 (1998).

²⁵A. Hernando *et al.*, Phys. Rev. B **51**, 3281 (1995).

²⁶P. Günber and D. Pierce, *Encyclopedia of Materials: Science and Technology* (Elsevier, Amsterdam, 2001).